ISSN 2089-8673 (Print) | 2548-4265 (Online)
Volume 14, Issue 3, 2025, pp. 597-615

OPTIMIZING SMALL-SCALE PUMPED HYDRO STORAGE OPERATION FOR OFF-GRID PV: MAXIMIZING STORED ENERGY UNDER LPSP AND CARBON FOOTPRINT CONSTRAINTS

Akhmad Musafa[1,3], Ardyono Priyadi[1], Vita Lystianingrum[1], Mauridhi Hery Purnomo[1,2, *]

[1]Department of Electrical Engineering, Institut Teknologi Sepuluh Nopember, Surabaya, Indonesia
[2]Department of Computer Engineering, Institut Teknologi Sepuluh Nopember, Surabaya, Indonesia
[3]Department of Electrical Engineering, Universitas Budi Luhur, Jakarta, Indonesia

Abstract

This study explores the utilization of Particle Swarm Optimization (PSO), Grey Wolf Optimization (GWO), and Puzzle Optimization Algorithms (POA) methodologies to improve the performance of a small-scale PHS integrated in an off-grid PV system in a building. The optimization objective function is to minimize the LPSP value, with a carbon footprint of less than 10 kg/kWh. The LPSP value is related to the total energy deficit and total load, and the carbon footprint value is related to the total heat generated by the PHS pump, generator, and carbon intensity value. The optimization setup uses a multi-objective function that has been simplified into a single weighted objective function with normalized and justified weights. The case study is conducted on a 5 kW PV system in a building with a water level of 24 meters and a PHS reservoir of 5 m^3. The system is tested under two conditions, namely during the rainy season (January) and the dry season (August). The PSO and GWO algorithms, based on testing results in January and August, demonstrated better performance than POA. This is based on the higher average total PHS energy compared to POA, as well as lower LPSP, LOLE, and EENS values. Meanwhile, for the average stored energy and carbon footprint values, the POA algorithm performs better than PSO and GWO, as indicated by the higher average stored energy and lower carbon footprint values.

Keywords: Carbon footprint, energy storage, optimization, photovoltaic, pumped hydro storage.

Received: 01-08-2025 | **Accepted:** 31-10-2025 | **Available Online:** 30-11-2025
DOI: https://doi.org/10.23887/janapati.v14i3.102327

I. INTRODUCTION

A. The Background of the Research

Based on data in [1], the average demand rate for electrical energy in Indonesia in the period from 2018 to 2050 is projected to be 7%. To meet the need for electrical energy nationally, it is supplied from the electrical energy generation system with fossil fuels, thus contributing carbon emissions (CO_2) of 44%-47% of the total carbon emissions, as presented in Figure 1.

Photovoltaic (PV) systems are one of the alternative electrical energy harvesting devices that are widely used both on a large scale in industry and on a small scale in buildings. The utilization of PV systems is driven by the objective of diminishing reliance on fossil fuels so that it can reduce carbon production [2]. However, the use of PV systems also requires energy storage devices, which generally use batteries, which in the long term can also potentially produce B3 waste (Toxic and Hazardous Materials), produce carbon and pollute the environment.

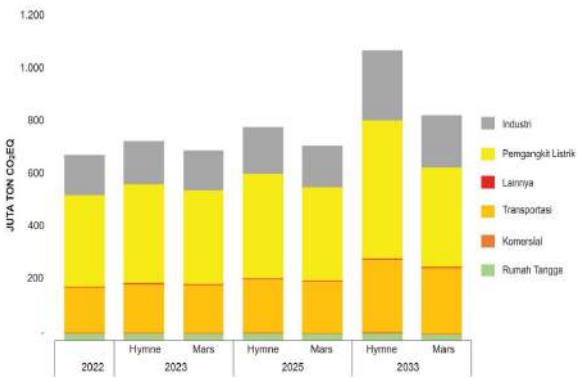

Figure 1. Carbon emissions (CO_2) by sector [1]

*Corresponding author: hery@ee.its.ac.id (M. H. Purnomo)

Therefore, the pumped hydro storage (PHS) systems is one of the alternative energy storage system options that is more environmentally friendly. Generally, on the rooftop of high-rise buildings there are water storage tanks that can be used as energy storage in the PHS system. For this reason, the PHS system can be the right choice as an energy storage system for PV systems in environmentally friendly buildings and has a long service life [3].

Research has previously been conducted on the use of PHS as an energy storage medium within renewable energy systems, with a particular focus on remote island communities [4]. Reference [5] also provides a review and future prospects for the use of PHS as an energy storage solution for hybrid photovoltaic and wind turbine systems. The use of PHS for energy storage in PV systems in remote areas also discussed in [6]. As demonstrated in extant research, the PHS system was developed for utilization in electric power systems characterized by large capacities (MW order).

The utilization of PHS as a medium for energy storage on a small scale, particularly within the context of buildings, is proposed in reference [7]. However, research results show that PHS systems in buildings are not economically feasible, because storing large amounts of energy requires large amounts of water storage. This is a challenge for further research on the optimal PHS system design for application in buildings and its feasibility analysis, both technically and economically, because in terms of its life cycle, PHS is the recommended energy storage system for use.

In another study [8], the PHS system as an energy diversion in a PV system connected to the grid in apartment buildings and villas was analyzed for its technical and economic feasibility. The findings of this study suggest that a PV system integrated with PHS has the potential to meet the energy demands of residential properties, thereby reducing the reliance on the power grid.

As an energy storage system, PHS systems still have a carbon footprint, although it is lower than that of other energy storage systems. On a large scale, the carbon footprint of PHS is related to its construction and operation. The carbon footprint is primarily attributable to the concrete utilized in the construction of the dam, in conjunction with the energy demands associated with the pumping of water uphill.

In small-scale applications, the carbon footprint is caused by the use of pumps and generators. The carbon footprint in this case is related to the efficiency of the pump and generator.

B. Related Works

Several previous studies on optimizing renewable energy system operations have been conducted. In paper [9], K. Sun et al. discussed the optimal combination operation scheme of PV-WT-PHS system. The multi-terminal HVDC based on VSCC acts as a link between the system parts. The present paper elucidates the automatic control function of PHS, which has been demonstrated to effectively reduce or compensate the deviation of PV-WT system output power from the estimated production value.

In paper [10], optimization of hydro thermal power plant scheduling is discussed to operate economically using the Artificial Bee Colony (ABC) method. In paper [11], application of the Improved Multi-Objective Crow Search Algorithm (IMCSA) method for optimization of smart grid operations is discussed. The optimization aims to improve the Available Efficiency Index (AEI), minimize power losses in the micro-grid system, and increase the availability, reliability, and benefits of the smart grid system.

Furthermore, in paper [12], the optimization of the operation of a combined PV-diesel generator-PHS system is discussed, using the modified Crow Search Algorithm (CSA) method. Optimization is only carried out to reduce diesel fuel consumption, and the technical-economic analysis has not been carried out. Reference [13] proposed the Pareto Frontier and e-constraint methods for operational optimization of a a community energy storage system, but has not taken into account optimization to maximize the stored energy in the energy storage system. Besides, optimization of distributed energy management in multi-energy generation networks (MEGG) can be done using a three-layer method based on a multi-agent system (MAS). Optimization aims to minimize emissions and system operating costs [14].

Previous research related to energy management systems is discussed in paper [15], where the energy management system for PV-PHS systems based on data forecasting results with ANN combined with a real-time controller is implemented in a farmhouse. The study results show that the scheduling method has poor performance when conditions are cloudy. Energy management optimization of the PV-PHS-Battery system utilizing rainfall harvesters using the PSO method to minimize the cost of component requirements and safe and reliable power supply management, so that the LSPP value is equal to zero, is discussed in paper [16]. The method proposed in this paper does not take into account

the predicted value of the energy source power and load.

In paper [17], the energy management of a micro-grid system is discussed. The method used is multi-agent system (MAS) model consisting of three layers: i.e. DMS, MGCC, and MGCE agents. Analysis of three cases, including energy storage systems used and distributed generation. The algorithm used for optimization is Adaptive Weighted and Chaotic PSO (ACPSO). Furthermore, in [18], a study is conducted on energy management in a micro-grid with droop control for distributed generation and frequency response that guarantees all techno-economic aspect constraints. Droop control model with gain as a time-dependent variable that is adaptive. Frequency response model of load based on thermostat-controlled load characteristics. Improvement of the cost effectiveness of energy management, carried out by coordination of time-varying gain determination of controllable distributed generation with frequency-responsive load.

Paper [19] propose optimization of the size and operation of a PHS system. The PHS system optimized was interacting with a hybrid power generation system. The purpose of this work is to identify the optimal size and operation strategy of a PHS plant. Two algorithms used are a surrogate modelling optimization algorithm and a mixed integer linear programming algorithm.

In paper [20] a low-carbon optimal scheduling method of a thermal battery PV-WT-PHS system with CHP is proposed with the aim of coordinated multi-energy complementarity of the hybrid energy system. Numerical simulation used to validate this method, and then use simulation results of the traditional optimal scheduling method without considering PHS and carbon trading as comparison.

The solution of multi-objective problems on the optimal operation of a hybrid system consisting of pumped hydro storage, cascade hydropower stations, run-of-river hydropower stations, and photovoltaic power plants is proposed in the paper [21]. The method used is the improved normal limit intersection (NBI) method. The maximization of the effective load-carrying capacity (ELCC) and economic income of the hybrid system are the goals of this work. In addition, the big-M method and the integrated binary expansion method with the linearization transformation technique are also used simultaneously to ensure optimal results.

In paper [22], an optimization of a renewable energy micro-grid system consisting of wind turbines, photovoltaic solar panels, batteries, and pumped hydro storage in an isolated area is proposed. The optimization methods used are Grey Wolf Optimization (GWO), Moth Flame Optimization (MFO), and the Dragonfly Algorithm (DA). Some of the optimization objectives carried out are: minimizing the average cost of energy (LCOE) by considering the probability of loss of power supply (LOPSP), increasing system reliability, and limiting excess energy generation (Pex).

Furthermore, in [23] a study was conducted to optimize the energy management of a PV-wind turbine-hydro pump-battery system. The proposed system aims better to meet the thermal needs of buildings in semi-arid climates.

C. The Solution Offered

From the references that have been described, there are research gaps, including:

- Various proposed renewable energy systems are generally large-scale systems, although there are some small-scale systems that are applied in buildings.
- Most systems still use other energy sources that still require fuel such as diesel, or energy storage systems still use batteries, even though there is a PHS system. This results in the carbon footprint produced by the system still being high.
- Most of the proposed optimization methods have not taken into account the carbon footprint value.

Based on the existing research gap, the work proposed focused on optimizing the operation of a renewable energy system that only uses PV and PHS with the aim of increasing stored energy by considering the LPSP value and carbon footprint.

The main contributions made by this work are:

- C1: The system used is a small-scale PV-PHS system, which in the energy harvesting process, in addition to harvesting solar energy, also involves harvesting energy from rainfall.
- C2: The system is designed on a small scale for applications in high-rise buildings that adapt to the conditions of the existing water reservoir system.
- C3: The optimization method is carried out by calculating the LPSP value and carbon footprint to produce the maximum stored energy.

II. METHOD

The block diagram of the PHS system as energy storage for the PV system applied in a

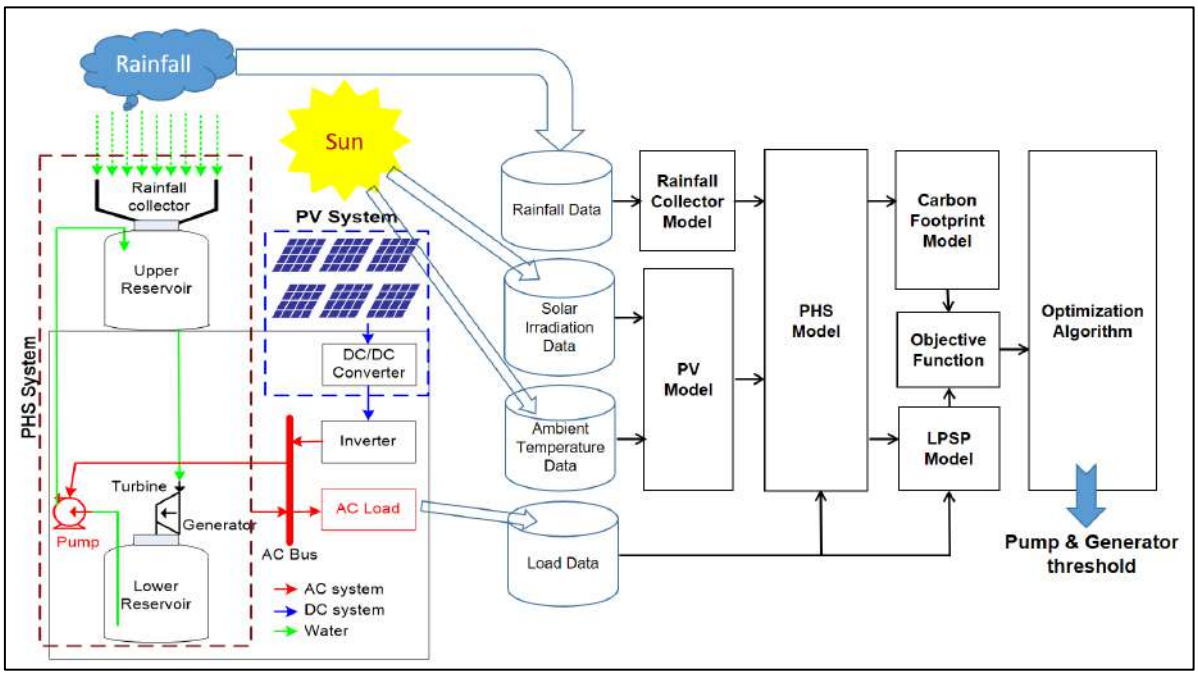

Figure 2. Block diagram of the PV-PHS system and the proposed PHS system operation optimization method.

high-rise building, and the optimization method for system operation proposed in this paper are shown in Figure 2. The system has been designed to be off-grid. The system under consideration consists of a PV array, a PHS system for the purpose of electrical energy storage, and a load. The specifications of the system parts used are delineated in Table 1.

Photovoltaic (PV) systems are designed to capture energy from sunlight. The output voltage of the PV system is input to the DC-DC converter, where it is converted to AC voltage using an inverter, and subsequently enters the AC bus. The initial utilization of AC power will be for the purpose of illuminating the building, with the objective of establishing a foundation for the subsequent operation of the system. The load value varies for each hour during a 24-hour period, exhibiting a consistent pattern on a daily basis.

Table 1. PV-PHS system specifications

Sub System	Parameters	Specification
PV System	PV capacity	5000 W
DC-DC converter	Gain	1
Inverter	Efficiency	88%
Upper Reservoir	Capacity	5 m^3 / 5000 liter
Lower Reservoir	Capacity	5 m^3 / 5000 liter
Generator	Power max	2000 W
	Efficiency	88%
Pump	Power	1000 W
	Efficiency	88%
Building Height	Head	24 m
Rainfall Collector	Catchment Area	4 m^2
Load	Min Load	50 W
	Max Load	1000 W

The surplus power generated by the PV system, subsequent to its utilisation for load supply, will be stored in the PHS system. The process of storage is facilitated by the utilisation of surplus power to operate the PHS pump, thereby ensuring the movement of water from lower to the upper reservoir. The water that enters the upper reservoir is sourced not only from the lower reservoir but also from rainwater collected through the rainwater collector. The potential energy that can be stored is determined by the volume of water stored in the upper reservoir, and then used to drive the turbine, which is coupled to the generator in the PHS system, where it will be converted into electrical energy. The PV power output will be combined with the output power of the PHS generator to supply the load. After supplying the load, if there is excess power, then the excess power is used to supply the PHS pump in the energy storage process again.

A. PV Power Model

The output power of a photovoltaic system is directly proportional to the installed photovoltaic capacity (PV_{cap} [W]), solar irradiation ($G(t)$ [W/m^2]), and the temperature of the photovoltaic cells ($T_{cell}(t)$ [ºC]). As demonstrated in (1), the cell temperature value is determined by the irradiation value and the ambient air temperature

value ($T_{amb}(t)$ [ºC]). Therefore, the photovoltaic output power can be calculated using (2).

$$T_{cell}(t) = T_{amb}(t) + \left(\frac{G(t)}{800}\right)(NOCT - 20) \quad (1)$$

$$P_{PV}(t) = PV_{cap}\left(\frac{G(t)}{G_{STC}}\right)\left(1 + k(T_{cell} - T_{TSC})\right) \quad (2)$$

B. Rain Collector Model

The rainwater collector installed above the PHS upper reservoirs is used to collect rainwater entering the upper reservoir. This is intended to guarantee that in instances where precipitation exceeds the capacity of the photovoltaic system to supply energy to the pump, the upper reservoir will still receive water, thereby ensuring the retention of stored energy within the PHS system. The volume of rainwater entering the rainwater collector ($V_R(t)$ [m^3]) is proportional to rainfall intensity ($R_R(t)$ [mm]) and the area of rainfall capture (A_R [m^2]), as demonstrated in (3).

$$V_R(t) = R_R(t) \cdot A_R \quad (3)$$

C. PHS Model

The PHS operates in two modes, i.e., pumping and generating. In the event of PHS operating in pumping mode, the energy-charging process is initiated (charging). Conversely, when PHS functions in generating mode, it results in the release of energy (discharging).

Mode of Pumping

If the PHS is operating in pumping mode, the PV power is utilized to facilitate the transfer of water from the lower reservoir to the upper reservoir. The water volume pumped to the upper reservoir ($V_p(t)$ [m^3]) is the result of the pump power ($P_p(t)$ [W]) multiplied by the pump efficiency (η_p), and divided by the product of the water density (ρ [kg/m^3]) multiplied by the height of the water flow pumped (h_p [m]), and the gravity coefficient (g [m/s^2]), as demonstrated in (4).

$$V_P(t) = \frac{\eta_P}{\rho \times g \times h_p} \cdot P_p(t) \quad (4)$$

The pump power ($P_p(t)$) can be varied in the following three conditions:

a) If $P_{PV}(t) > P_L(t)$, and $V_{UR}(t) > V_{LR}(t)$ then the pump power is:

$$P_P(t) = (P_{PV}(t) + P_G(t)) - P_L(t) \quad (5)$$

b) If $P_{PV}(t) > P_L(t)$, and $V_{UR}(t) \leq V_{LR}(t)$, then the pump power is:

$$P_P(t) = P_{PV}(t) - P_L(t) \quad (6)$$

c) If $P_{PV}(t) \leq P_L(t)$, and $V_{UR}(t) > V_{LR}(t)$ is , then the pump power is:

$$P_P(t) = P_G(t) - P_L(t) \quad (7)$$

Mode of Generation

In generation mode, the power output of the PHS generator (P_G [W]) is product of the volumetric flow rate of water from upper to lower reservoir(q_G[m^3/s]) with the generator efficiency (η_G), the density of water (ρ), the acceleration due to gravity (g) and the water fall height (h_G), as demonstrated in (8).

$$P_G(t) = q_G(t) \cdot \eta_G \cdot \rho \cdot g \cdot h_G \quad (8)$$

Upper and Lower Reservoir Model

In this work, the upper reservoir is designed by the addition of a rainwater reservoir above it. The objective is to ensure that the upper reservoir is capable of accommodating water that has been pumped from the lower reservoir, as well as rainwater during periods of precipitation.

The volume of the upper reservoir at a given time ($V_{UR}(t)$ [m^3]) is defined as the sum of the volume of the upper reservoir at the previous time ($V_{UR}(t-1)$ [m^3]), the volume of water pumped from the lower reservoir ($V_P(t)$ [m^3]), and the volume of incoming rainwater ($V_R(t)$ [m^3]), minus the volume of water discharged to the generator ($V_G(t)$ [m^3]). The mathematical model of the upper reservoir volume is shown in (9).

$$V_{UR}(t) = V_{UR}(t-1) + V_P(t) + V_R(t) - V_G(t) \quad (9)$$

Concurrently, the volume of the lower reservoir at a given moment ($V_{LR}(t)$ [m^3]) exhibits a direct proportionality to the sum of the volume of the lower reservoir at the previous moment ($V_{UR}(t-1)$ [m^3]), with the volume of water flowing into the lower reservoir ($V_G(t)$), minus the volume of water pumped into the upper reservoir ($V_P(t)$). The mathematical model of the upper reservoir volume is shown in (10).

$$V_{LR}(t) = V_{LR}(t-1) + V_G(t) - V_P(t) \quad (10)$$

Stored Energy

Based on the upper reservoir model in (9), the performance of the energy storage system in the PHS can be determined by calculating the State of Charge (SOC [%]) and stored energy in the PHS as shown in (11) and (12).

$$SOC_{PHS} = \frac{V_{UR}(t)}{V_{UR-cap}} \times 100\% \quad (11)$$

$$E_{PHS}(t) = \frac{V_{UR}(t) \times g \times h_G}{3600} \quad (12)$$

D. Problem Formulation

Reliability analysis

PV-PHS system is a power system that uses intermittent renewable energy sources. For this reason, the reliability of the system needs to be considered. The reliability of PV-PHS systems

can be evaluated by looking at several reliability indices, which are important points in the planning and operation of power systems. System reliability indices that need to be considered include the Loss of Power Supply Probability (LPSP [%]), Loss of Load Expectation (LOLE [hours]), and Expected Energy Not Supplied (EENS [kWh]). These three reliability indices are related to the energy deficit ($LPS(t)$) (13), expressed as (14), (15), and (16), respectively.

$$LPS(t) = P_L(t) - \left(P_{PV}(t) + P_{PHS}(t)\right) \quad (13)$$

$$LPSP = \frac{\sum_{t=1}^{n} LPS(t)\eta_{inv}}{\sum_{t=1}^{n} P_L(t)} \quad (14)$$

$$LOLE = \sum_{t=1}^{n} \begin{cases} 1, & LPS(t) > 0 \\ 0, & LPS(t) \leq 0 \end{cases} \quad (15)$$

$$EENS = \sum_{t=1}^{n} LPS(t) \quad (16)$$

Environmental Impact Analysis

In addition to system reliability, the PV-PHS system design must be evaluated to assess its environmental impact. The environmental impact referred to in this case is the carbon footprint value resulting from the operation of the PHS system pumps and generators. It is acknowledged that the operation of a pump and generator invariably generates heat, which is subsequently released into the ambient atmosphere. The heat energy produced by the pump ($ht_p(t)$[kWh]) and generator ($ht_g(t)$[kWh]) is influenced by the energy produced and their respective efficiencies, as demonstrated in (17) and (18).

$$ht_P(t) = E_P \times (1 - \eta_P) \quad (17)$$

$$ht_G(t) = E_G \times (1 - \eta_G) \quad (18)$$

The carbon footprint value (CF [kg CO_2e]) of the PHS system can be calculated using (19), which is based on the value of the heat energy produced by the pump and generator. CI [kg CO_2/kWh] is the carbon intensity value generated by the PHS systems.

$$CF(t) = CF(t-1) + \left(ht_P(t) + ht_G(t)\right) \times CI \quad (19)$$

Referring to [24], the value of the PHS system is that the carbon intensity for each kWh of energy supplied to the PHS system is 0.058 to 0.530 kg CO_2e/kWh. This value is a limitation in optimizing the operation of the PHS system related to the carbon intensity parameter.

Objective Function

The objective function of optimization is to minimize the loss of power supply probability (LPSP) and carbon footprint, while maximizing stored energy. The optimization setup employs a multi-objective function that has been simplified into a single weighted objective function with normalized and justified weights. The objective function equation is illustrated in (20).

$$F(X) = min(w_1 LPSP + w_2 CF) \quad (20)$$

Where X is the optimization result variable consisting of the threshold value of the pump and generator power capacity of the PV-PHS system when operating. w_1 and w_2 denote the weighting factors for LPSP and CF optimization, respectively, which are selected using a trial-and-error method.

$$X = \begin{bmatrix} P_p & P_G \end{bmatrix} \quad (21)$$

The constraints that must be considered in optimization are as follows:

$$P_p^{min} \leq P_P \leq P_P^{max} \quad (22)$$

$$P_G^{min} \leq P_G \leq P_G^{max} \quad (23)$$

$$LPSP \leq LPSP_{max} \quad (24)$$

P_P^{min} and P_P^{max} represent the minimum and maximum power capacity of the pump, P_G^{min} and P_G^{max} represent the minimum and maximum power capacity of the generator.

The objective function is modified through the implementation of a progressive penalty system, wherein the penalty weight undergoes an increase with each iteration of the program (ranging from 50 to 500). In instances where the target LPSP is set at or below 10%, the penalty will be initiated if the LPSP value exceeds 10%. In this scenario, the objective function undergoes modification, as illustrated in (25) and (26). In this study, the minimum iteration value is denoted by w_{pen}, ranging from 50 to 500.

$$F(X) = 0.85\left(LPSP + LPSP_{pen}\right) + 0.15CF \quad (25)$$

$$LPSP_{pen} = w_{pen}(LPSP - 10) \quad (26)$$

E. Proposed Optimization Approach

Particle Swarm Optimization Algorithm

The PSO algorithm model is described in the paper. A particle is expressed as a point in a certain dimensional space that has two information parameters. These are the position of the i^{th} particle at the k^{th} iteration $\left(x_i^k\right)$ and the velocity of the i^{th} particle at the k^{th} iteration $\left(y_i^k\right)$. These are expressed by (27) and (28), respectively. Here, i is the iteration number (i^{th}

iteration), j is the particle index and N is the number of particles.

$$x_i^k = \left(x_{i,1}^k, x_{i,2}^k, \cdots, x_{i,N}^k\right) \quad (27)$$

$$v_i^k = \left(v_{i,1}^k, v_{i,2}^k, \cdots, v_{i,N}^k\right) \quad (28)$$

The process by which the position $\left(x_i^{k+1}\right)$ and velocity $\left(v_i^{k+1}\right)$ status of a particle is updated is articulated through (29) and (30).

$$x_i^{k+1} = x_i^k + v_i^{k+1} \quad (29)$$

$$v_i^{k+1} = \omega v_i^k + c_1 r_1\left(\boldsymbol{pbest}_i^k - x_i^k\right) + c_2 r_2\left(\boldsymbol{gbest}_i^k - x_i^k\right) \quad (30)$$

In this model, the inertia weight coefficient is denoted by ω, while the cognitive coefficient c_1 and social coefficient c_2 are utilized to accelerate the search process. The random real numbers r_1 and r_2 are constrained to the interval [0,1]. Each particle is best denoted as $pbest_i^k$. If the subsequent particle fitness value is not superior to the preceding $k+1$ iterations, it can be deduced that the value of $pbest_i^{k+1}$ is equivalent to the value of $pbest_i^k$. $gbest_i^k$ demonstrates the value of the optimal group (swarm). If the fitness value of the subsequent optimal group is not superior to that of the preceding $k+1$ iterations, the value of $gbest_i^{k+1}$ is equivalent to that of $gbest_i^k$.

Grey Wolf Optimization Algorithm

The Grey Wolf Optimization (GWO) algorithm was introduced by Seyedili Mirjalili in 2014 [25], which works using the concepts of hunting, social hierarchy, and leadership structure of grey wolves in nature. The GWO algorithm has four solution structures; the first is alpha (α) as the best solution, the next level is beta (β) as the second solution, then delta (δ) is the third solution, and the last solution is omega (ω). To get the best solution, the GWO algorithm has 3 stages, i.e., 1) encircling the prey, 2) hunting the prey, and 3) attacking the prey.

In the first step, grey wolves encircle the prey by following (31) and determine the prey location using (32). $\vec{X}$ and $\vec{X}_p$ are the positions of the grey wolves and the targeted prey. $\vec{A}$ and $\vec{C}$ are coefficient vectors obtained using (33) and (34). r_1 and r_2 are random numbers from 0 to 1, and $\vec{a}$ is set vector value 2 to 0 decreases linearly as iteration increases.

$$\vec{D} = \left|\vec{C} \cdot X_p(t) - \vec{X}(t)\right| \quad (31)$$

$$\vec{X}(t+1) = \vec{X}_p(t) - \vec{A} \cdot \vec{D} \quad (32)$$

$$\vec{A} = 2\vec{a}\,\vec{r_1} - \vec{a} \quad (33)$$

$$\vec{C} = 2\vec{r_2} \quad (34)$$

In the second step, the grey wolf group updated their positions according to the key group to get the best solutions. Equations (35) – (38) represent the position of each wolf in the group, where $\overrightarrow{X_\alpha}$, $\overrightarrow{X_\beta}$, and $\overrightarrow{X_\delta}$ are the three best solutions during the iterative procedure. While $\vec{D}$ is a coefficient vector determined using (39) – (41).

$$\vec{X}(t+1) = \frac{\vec{X}_1 + \vec{X}_2 + \vec{X}_3}{3} \quad (35)$$

$$\vec{X}_1 = \vec{X}_\alpha - \vec{A}_1\vec{D}_\alpha \quad (36)$$

$$\vec{X}_2 = \vec{X}_\beta - \vec{A}_2\vec{D}_\beta \quad (37)$$

$$\vec{X}_3 = \vec{X}_\delta - \vec{A}_3\vec{D}_\delta \quad (38)$$

$$\vec{D}_\alpha = \left|\vec{C}_1\vec{X}_\alpha - \vec{X}\right| \quad (39)$$

$$\vec{D}_\beta = \left|\vec{C}_1\vec{X}_\beta - \vec{X}\right| \quad (40)$$

$$\vec{D}_\delta = \left|\vec{C}_1\vec{X}_\delta - \vec{X}\right| \quad (41)$$

In the third step, the grey wolf attacks its prey when the prey stops moving, and the hunting process stops. This condition is mathematically expressed by (42), where t represents an integer value from 0 to the maximum iteration value t_{max}.

$$a = 2\left(1 - \frac{t}{t_{max}}\right) \quad (42)$$

Puzzle Optimization Algorithm

The Puzzle Optimization (POA) algorithm was first proposed by [26] in 2021 to resolve a variety of optimization problems. The fundamental concept underpinning the design of the proposed POA is a mathematical simulation of the process of solving a puzzle as an evolutionary optimizer.

The POA algorithm has been developed on the basis of a puzzle game simulation. In POA, a population-based game algorithm, each member of the population is a feasible solution to the optimization problem. The values of the problem variables are determined by each member of the population. Equation (43) illustrates the population model in POA.

$$X = \begin{bmatrix} X_1 \\ \vdots \\ X_i \\ \vdots \\ X_N \end{bmatrix}_{N\times m} = \begin{bmatrix} x_{1,1} \cdots x_{1,d} \cdots x_{1,m} \\ \vdots \ \ddots \ \vdots \ \iddots \ \vdots \\ x_{i,1} \cdots x_{i,d} \cdots x_{i,m} \\ \vdots \ \ddots \ \vdots \ \iddots \ \vdots \\ x_{N,1} \cdots x_{N,d} \cdots x_{N,m} \end{bmatrix}_{N\times m} \quad (43)$$

In the context of the problem under consideration, X denotes the puzzle population, X_i designates the i_{th} puzzle, N signifies the number of puzzle populations, m represents the

number of problem variables, and $x_{(i,d)}$ refers to the values suggested by the i_{th} puzzle for the d_{th} variable. The objective function value (F) is evaluated, whereupon the obtained objective function value is simulated using the vector in (44), f_i is the value of the objective function of the i_{th} puzzle.

$$F = \begin{bmatrix} f_1 \\ \vdots \\ f_2 \\ \vdots \\ f_N \end{bmatrix}_{N\times 1} = \begin{bmatrix} F(X_1) \\ \vdots \\ F(X_i) \\ \vdots \\ F(X_N) \end{bmatrix}_{N\times 1} \quad (44)$$

A comparison will be made of the values obtained for the objective function. The member that provides the optimal value for the objective function is designated as the most outstanding member of the population, a determination that can be made using (45). In (45), B is identified as the optimal member, while X_k represents the k_{th} puzzle, characterized by a minimum objective function value of f_k.

$$B = min(F) = X_k, f_k \quad (45)$$

In the POA algorithm, the population members are updated in two stages. In the first stage, each member of the population is updated based on the suggestions of other members, which is modeled mathematically in (46) - (50).

$$GM_i = X_g, \quad g \in \{1,2,3\cdots,N\} \quad (46)$$

$$dx_{i,d} = \begin{cases} \left(GM_{i,d} - I \times x_{i,d}\right), F_g < F_i \\ x_{i,d} - I \times GM_{i,d}, else \end{cases} \quad (47)$$

$$I = round(1 + rand) \quad (48)$$

$$X_i^{new} = X_i + r \times dX_i \quad (49)$$

$$X_i = \begin{cases} X_i^{new}, & F_i^{new} < F_i \\ X_i, & else \end{cases} \quad (50)$$

In the subsequent phase, designated as the second stage, the status of each population member will be updated through the utilization of puzzle pieces proposed by other members of the population. The mathematical underpinnings of this stage are delineated in (51) to (53).

$$N_P = round\left(0.5 \times \left(1 - \frac{t}{T}\right) \times N\right) \quad (51)$$

$$X_{i,d_j}^{new} = X_{h,d_j}, = \begin{cases} h & \in \{1,2,3,\cdots,N\} \\ j & \in \{1,2,3,\cdots,N\} \\ d_j & \in \{1,2,3,\cdots,N\} \end{cases} \quad (52)$$

$$X_i = \begin{cases} X_i^{new}, & F_i^{new} < F_i \\ X_i, & else \end{cases} \quad (53)$$

From (49) to (51), N_P signifies the quantity of proposed puzzle pieces, t denotes the iteration counter, T represents the maximum number of iterations, and X_{i,d_j}^{new} is the new value for the d_j,th dimension of the i'th puzzle, and X_{h,d_j} is the suggested puzzle piece selected from the h'th puzzle, with h being randomly selected.

The subsequent iteration of the algorithm and determination of the new status of the population members is conducted only after the completion of the updating of all population members according to the first and second stages. The result of POA will present the best quasi-optimal solution to the optimization problem after the completion of the algorithm iteration.

III. RESULT AND DISCUSSION

The system optimization testing proposed in this paper was carried out by applying three optimization algorithms: the Particle Swarm Optimization (PSO) algorithm, the Grey Wolf Optimization (GWO) algorithm, and the Puzzle Optimization Algorithm (POA). Testing was conducted using a dataset of solar irradiation, ambient temperature, and rainfall in Universitas Budi Luhur environment, Jakarta, Indonesia, with coordinates of 6.240° South Latitude and 106.750° East Longitude. The dataset under consideration has a sampling time of 60 minutes, with the period spanning from 1 January 2020 to 31 December 2023. The dataset was obtained from the NASA Prediction of Worldwide Energy Resources page.

Testing was conducted in two scenarios: the first scenario was testing in the month representing the rainy season, namely January 2023, while the second scenario was testing in the month representing the dry season, namely August 2023. Each scenario was subjected to a rigorous testing process involving 744 datasets, encompassing irradiation, ambient temperature, and rainfall parameters. The optimization results of these three algorithms will be compared with the initial test results without optimization (baseline condition). The system parameters employed in the testing process are delineated in Table 1. The initial condition posits that the water volumes in the upper and lower reservoirs are 50% of their respective maximum capacities, totaling 2500 liters.

A. First Scenario: Testing During the Rainy Season

In the first scenario, testing was conducted in January 2023, which corresponded to the characteristics of the rainy season, with an average irradiance of 178 W/m2, an ambient temperature of 27 °C, and a rainfall of 0.23 mm.

Baseline Condition of First Scenario

The simulation results of baseline conditions (i.e., the system is not optimized) show an average PV power of 422.30 watts and an average PHS generator power of 11.26 watts. The total energy generated by the PV system and PHS generator in January of 2023 was 314,189 kWh and 8,376 kWh, respectively. Therefore, the total stored energy during January was 77,048 kWh, with a total load energy of 291.4 kWh. System reliability metrics revealed a Loss of Power Supply Probability (LPSP) of 25.01%, Loss of Load Expectancy (LOLE) of 540 hours, and Expected Energy Not Supplied (EENS) of 82,831 kWh. Regarding environmental impact, the operation of the PV-PHS system under baseline conditions resulted in a carbon footprint of 1.99 kgCO2e. The pump threshold and the generator threshold are equivalent to the baseline conditions of the first and second scenario tests, which are 100 watts each. Figure 3 presents sample profiles of key variables, including irradiation, ambient temperature, rainfall, power, reservoir volume, PHS state of charge (SOC), pump and generator status, PHS power and stored energy, LPSP, and carbon footprint, collected during the fifth week of January (January 29 - 31, 2023).

As illustrated in Figure 3, in instances where the photovoltaic (PV) power output exceeds the load power requirements, the surplus energy is utilized to satisfy the load demand. After the provision of power to the load, the residual energy is allocated to the operation of the PHS water pump, which facilitates the transfer of water from the lower reservoir to the upper reservoir. In this scenario, the PHS functions in pumping mode. The activation of the water pump has been demonstrated to result in an escalation in the carbon footprint, concomitant with an increase in the LPSP value.

Otherwise, when the PV power output is less than the load power requirement, and the upper reservoir volume exceeds the lower reservoir volume, the PHS will operate in generation mode. Consequently, the PHS generator will remain active until the water in the upper reservoir is depleted. As a result, when the PHS generator is operating, the carbon footprint value will increase, while the LPSP value will decrease. The integration of a PV power with a PHS generator is a strategic measure employed to ensure the fulfillment of electrical demands. Suppose the aggregate power output of the PV system and the PHS generator is insufficient to satisfy the load demand. In that case, the system enters a state of deficit, also referred to as "unmet load." Conversely, in the event that the PV and PHS generators are capable of meeting the requisite demand, the unmet load will decrease accordingly.

Optimization Results of First Scenario

Subsequently, system optimization is conducted employing the PSO, GWO, and POA methodologies, with parameter values for each of the three optimization algorithms presented in Table 2. Each optimization algorithm was run 20 times in multiple runs. This was done to strengthen the robustness of each algorithm's testing and achieve the best fitness value. The results of the convergence analysis of the optimization algorithm testing with PSO, GWO, and POA with 50 agents, 50 iterations, and multiple runs 20 times are presented in Figure 5.

From Figure 5, it can be seen that optimization with the PSO algorithm, with multiple runs of 20 times, the mean fitness value is achieved at 634.1540 with a standard deviation value of 0.0050, while the minimum and maximum values are 634.1484 and 634.1585, respectively. For the GWO algorithm, the mean fitness value is 634.1520 with a standard deviation of 0.0048, with the minimum and maximum values being 634.1484 and 634.1585, respectively. Meanwhile, for the optimization results with the POA algorithm, the mean fitness value is achieved at 663.7579 with a standard deviation value of 18.0261, while the minimum and maximum values are 634.8126 and 709.8301, respectively. The box plot depicting the comparison of the average fitness convergence value with the standard deviation of the PSO, GWO, and POA algorithms is presented in Figure 7.

Table 2. Parameters of PSO, GWO, and POA Algorithms

Parameter	PSO	GWO	POA
Population (*Np*)	50	50	50
Max Iterations	50	50	50
Parameters	w = 0.9-0.7(Iteration/Max Iteration) c_1 = 2.5-1(Iteration/Max Iteration) c_2 = 1.5+1(Iteration/Max Iteration)	a = 2 – Iteration(2/Max Iteration)	F_i = 0.7 – 0.4(Iteration / Max Iteration)

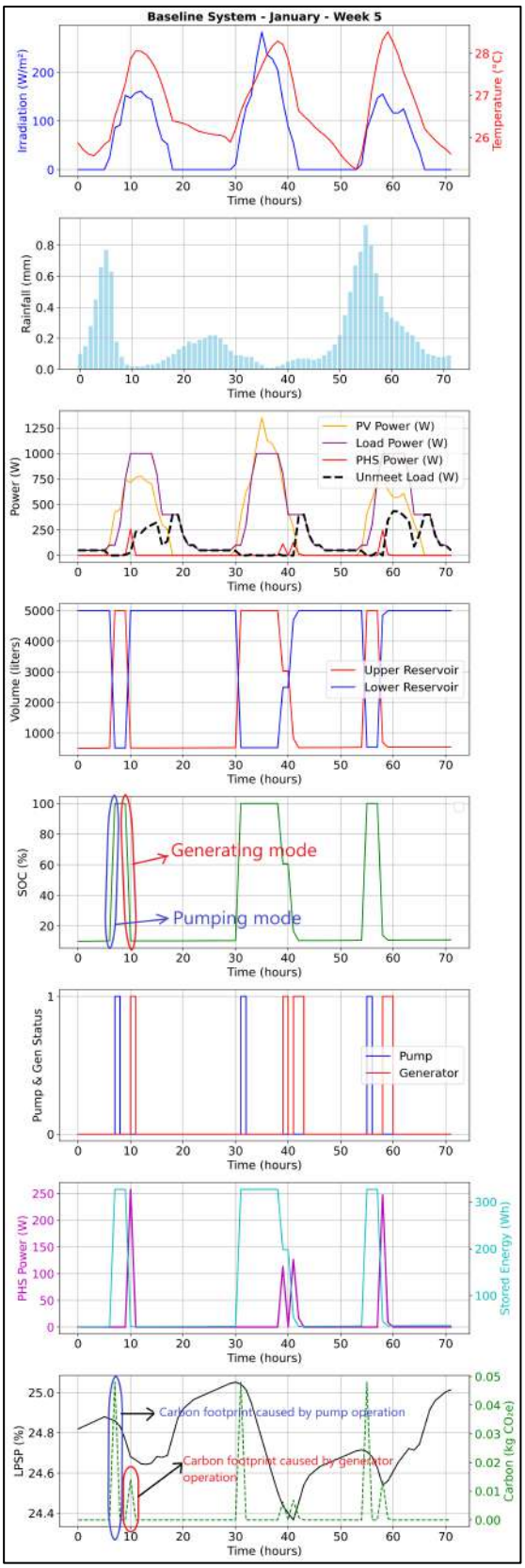

Figure 3. Parameter profile of small-scale PV-PHS system under baseline condition in the fifth week of January (January 29 - 31, 2023)

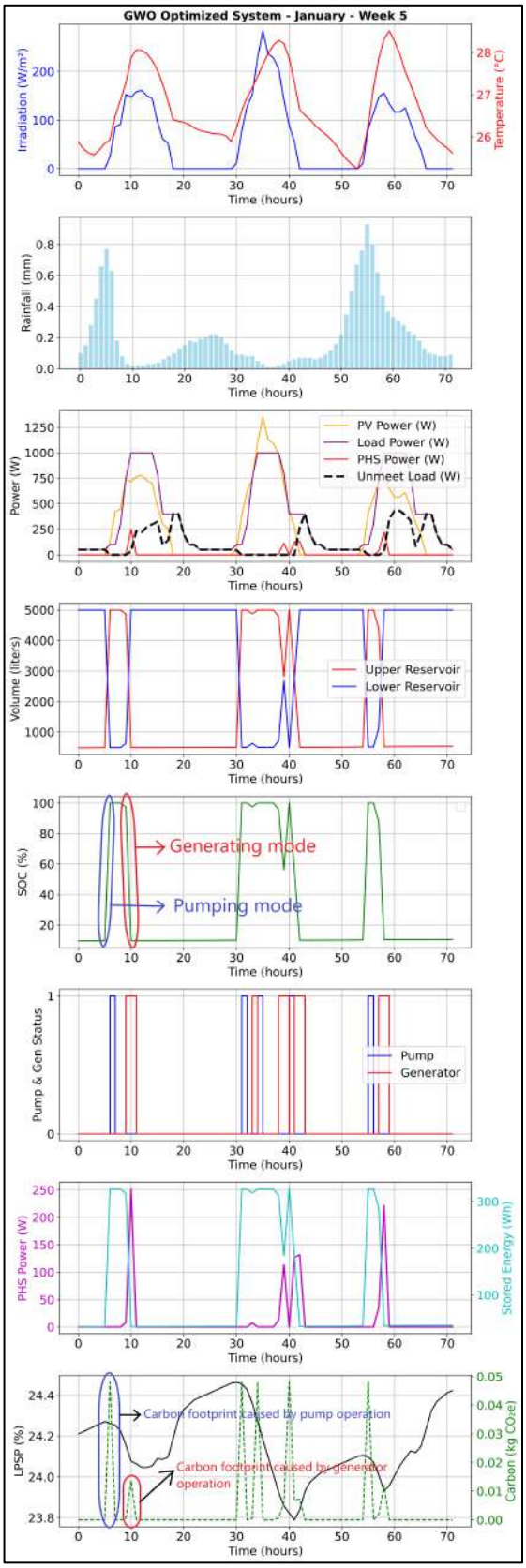

Figure 4. Parameter profile of small-scale PV-PHS system resulting from GWO algorithm optimization in the fifth week of August (August 29 - 31, 2023)

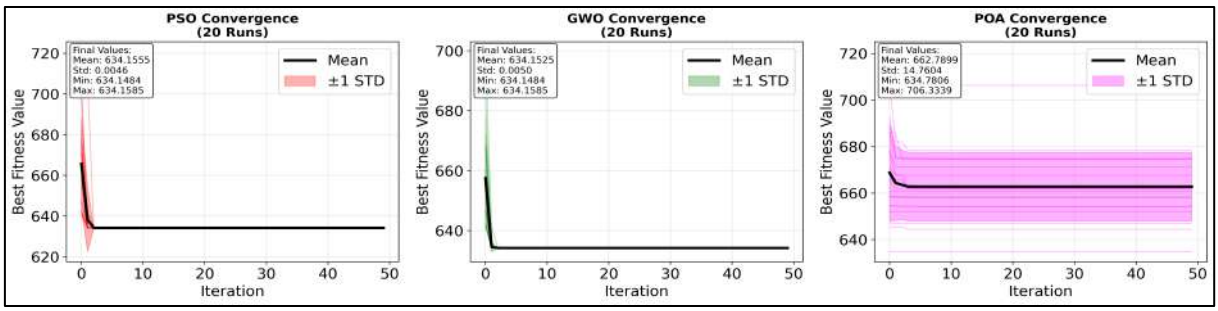

Figure 5. Comparison of the best fitness values of the PSO, GWO, and POA algorithms in optimizing the operation of a small-scale PV-PHS system in January 2023

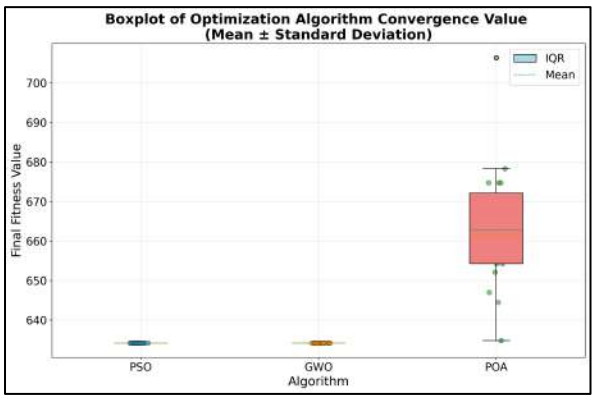

Figure 6. Boxplot of optimization convergence value (mean ± standard deviation) using PSO, GWO, and POA algorithms in optimizing the operation of a small-scale PV-PHS system in January 2023

Statistical Analysis of First Scenario

To further analyze the relative performance of the three algorithms, statistical analysis was conducted using the Wilcoxon Signed-Rank Test and the Mann-Whitney U Test. The present analysis compared the PSO algorithm with GWO, as well as PSO with POA. The results of this statistical analysis are presented in Table 3 and Table 4.

Table 3. Wilcoxon Signed-Rank Test Analysis for 1st Scenario

Parameters	Comparison Algorithm		
	PSO-GWO	PSO-POA	GWO-POA
Wilcoxon Statistic	9.000000	0.000000	0.000000
P-Value	0.157299	0.000088	0.000088
Significant	No	Yes	Yes
Better Algorithm	GWO	PSO	GWO
Median	PSO= 634.158522 GWO= 634.148413	PSO= 634.158522 POA= 664.453403	GWO= 634.148413 POA= 664.453403

As demonstrated in Table 3, an analysis of the data reveals that there is no statistically significant difference between the PSO and GWO algorithms (p-value = 0.157 > 0.05). However, the GWO algorithm is regarded as superior to the PSO algorithm, with a median value of 634.148413, as compared to the PSO algorithm's median value of 634.158522. Consequently, the GWO algorithm demonstrates enhanced stability and efficiency in the context of evaluating the optimization of this small-scale PV-PHS system.

Meanwhile, in the comparison of PSO with POA, there is a significant difference marked by p-value = 0.000088 < 0.05. With a PSO median of 634.158522, much lower than the POA median (664.453403), PSO is proven to be significantly superior to POA. In this context, PSO is superior compared to POA.

Similarly, in the comparison between the GWO and POA algorithms, there is a significant difference marked by p-value = 0.000088 < 0.05. It is clear that the GWO algorithm is better than the POA algorithm. The GWO median is 634.148413, much lower than the POA median of 664.453403. The GWO and PSO algorithms have statistically equivalent performance, but GWO is slightly superior. In the context of this proposed optimization, the POA algorithm is significantly inferior to the PSO and GWO algorithms.

Table 4. Mann-Whitney U Test Analysis for 1st Scenario

Parameters	Comparison Algorithm		
	PSO-GWO	PSO-POA	GWO-POA
Mann-Whitney	1.082004	5.410018	5.410018
P-Value	0.279251	0.000000	0.000000
Significant	No	Yes	Yes
Better Algorithm	GWO	PSO	GWO

In the Mann-Whitney U Test analysis, in the first comparison (PSO-GWO), there was no statistically significant difference between the performance of the PSO and GWO algorithms. While GWO demonstrated a marginal superiority in the ratings, this discrepancy was not deemed to be statistically significant at the 95% confidence level. In addition, a substantial discrepancy was identified between PSO and POA in the second comparison (PSO-POA).

PSO has been demonstrated to be statistically superior to POA with a very high level of confidence. The GWO-POA comparison yielded analogous results to the PSO-POA comparison, wherein GWO exhibited a substantial superiority over POA, accompanied by a highly statistically significant discrepancy.

The optimization results with the PSO algorithm demonstrate that with an average PV power of 422.30 watts and an average load power of 391.67 watts, the average PHS generator power is 13,887 watts. Consequently, the total energy produced by the PHS generator is 10.332 kWh, and the total stored energy is 80,584 kWh. The PSO algorithm was employed to optimize the process, resulting in a 25.01% reduction in the baseline LPSP to 24.42%. This reduction led to a concurrent decrease in the LOLE value from 540 to 524 hours and the EENS value from 82.831 kWh to 80.875 kWh. Additionally, the carbon footprint was reduced from 2.53 kgCO2e, signifying a significant environmental benefit. In terms of optimization with the GWO algorithm, the overall performance is equivalent to that of the PSO algorithm.

Conversely, optimization with the POA algorithm showed inferior performance compared to optimization results with the PSO and GWO algorithms. This is consistent with the results of statistical analysis using the Wilcoxon Signed-Rank Test and the Mann-Whitney U Test.

The average PHS power generated from the POA algorithm optimization is 12,566 watts, with a total stored energy of 82,266 kWh. The system reliability metrics show an LPSP value of 24.72%, a LOLE of 542 hours, and an EENS of 81,859 Wh. The carbon footprint value of the optimization results with the POA algorithm is lower than the PSO and GWO algorithms. Parameter profile of small-scale PV-PHS system resulting from GWO algorithm optimization in the fifth week of January 2023, as shown in Figure 4. Comparative data on the performance of the small-scale PV-PHS system under baseline conditions and optimization results in the initial scenario, carried out in January 2023, representing the characteristics of the rainy season, are presented in Table 5.

B. Second Scenario: Testing During the Dry Season

In the second scenario, testing was conducted in August 2023, which corresponded to the characteristics of the dry season, with an average irradiance of 372 W/m2, an ambient temperature of 27.12 °C, and a rainfall of 0.02 mm.

Baseline Condition of Second Scenario

In August of 2023, the small-scale PV-PHS system was subjected to testing under baseline conditions. The results of this testing indicated an average PV power value of 858.76 watts, an average PHS generator power of 12.41 watts, and an average load power of 391.67 watts. In conditions of higher irradiation than were observed in January, the photovoltaic system and the photovoltaic-hydrogen system were capable of producing a total energy output of 638,917 kilowatt-hours and 9,231 kilowatt-hours, respectively. Concurrently, the total energy stored during August amounted to 115,366 kWh.

The system reliability metrics in the August test exhibited a lower Loss of Power Supply Probability (LPSP) value compared to January, specifically 13.70%, with a Loss of Load Expectancy (LOLE) value of 399 hours and an Expected Energy Not Supplied (EENS) value of 45,374 kWh. In regard to the environmental impact, the augmented energy production led to a heightened carbon footprint value of 2.09 kgCO2e. The performance parameter profile of the PV-PHS system under baseline conditions during the test conducted in the fifth week of August 2023 (August 29 - 31, 2023) is illustrated in Figure 7.

Optimization Results of Second Scenario

As was the case in the initial scenario, subsequent to the evaluation of the baseline conditions, the subsequent step is to optimize the operation of the small-scale PV-PHS system. This will be achieved through the utilization of the PSO, GWO, and PO algorithms, with the parameters for the three optimization algorithms as presented in Table 2, and each optimization algorithm was run multiple 20 times.

Table 5. A comparative analysis of power, energy, and operating performance metrics of small-scale PV-PHS systems was conducted in January of 2023.

System	Total PV energy (kWh)	Total PHS energy (kWh)	Total Stored Energy (kWh)	LPSP (%)	LOLE (hours)	EENS (kWh)	Carbon ($kgCO_2e$)
Baseline	314.189	8.376	77.048	25.01	540	82.831	**1.99**
PSO	314.189	**10.332**	80.584	**24.42**	**524**	**80.875**	2.53
GWO	314.189	**10.332**	80.584	**24.42**	**524**	**80.875**	2.53
POA	314.189	9.349	**82.266**	24.72	542	81.859	2.19

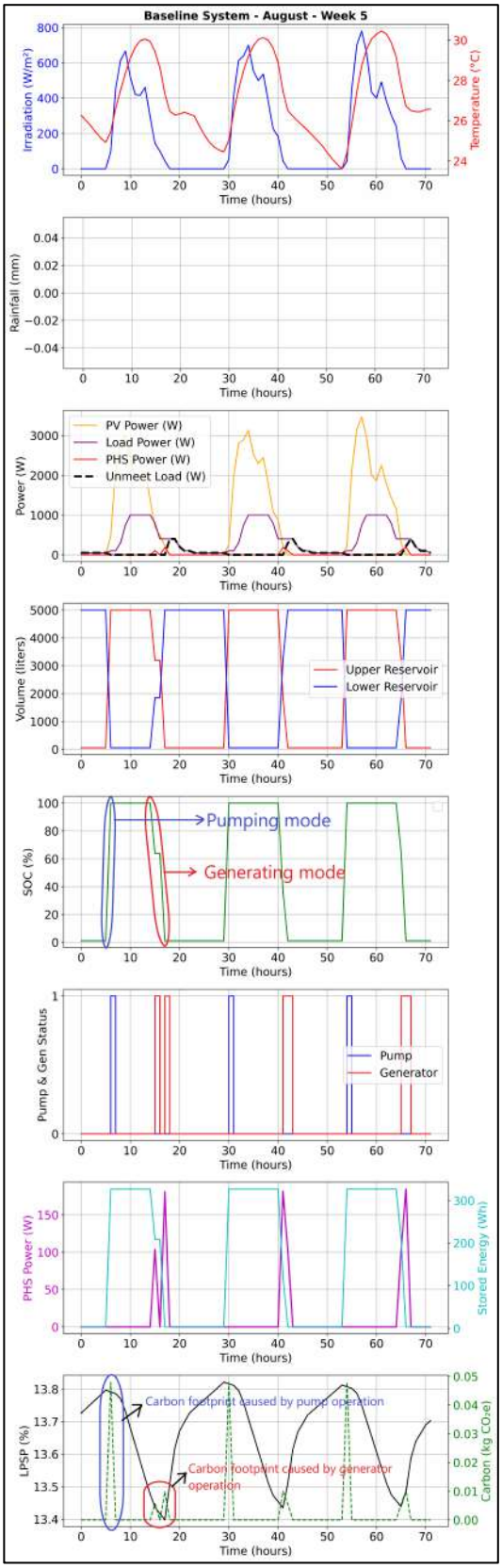

Figure 7. Parameter profile of small-scale PV-PHS system under baseline condition in the fifth week of August (August 29 - 31, 2023)

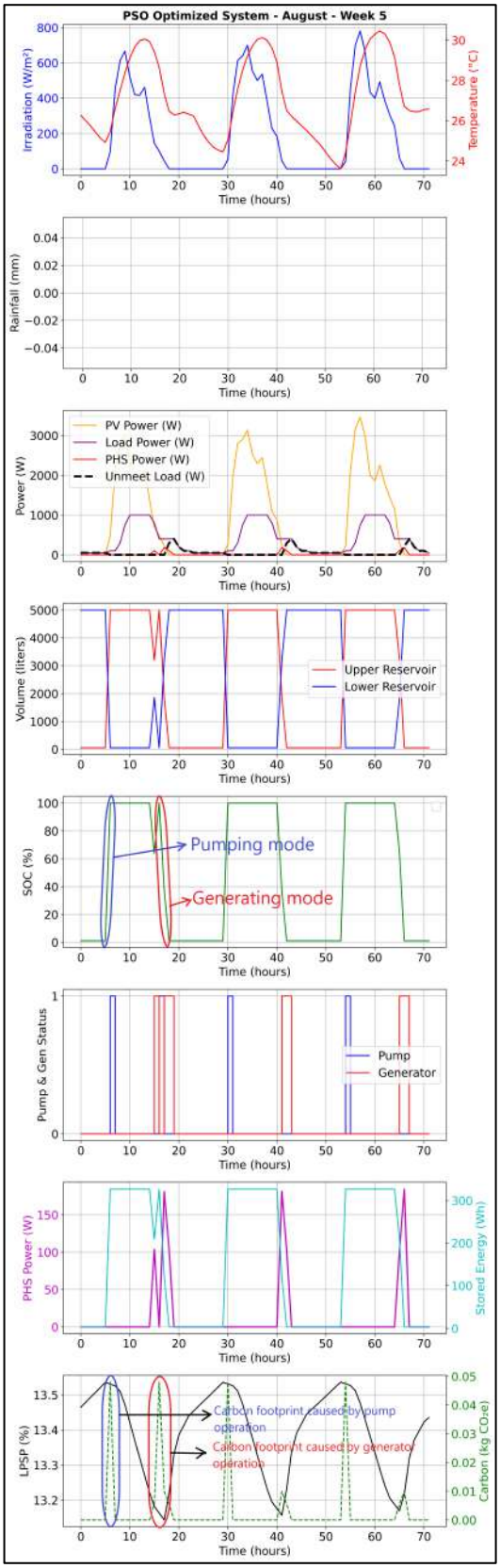

Figure 8. Parameter profile of small-scale PV-PHS system resulting from PSO algorithm optimization in the fifth week of August (August 29 - 31, 2023)

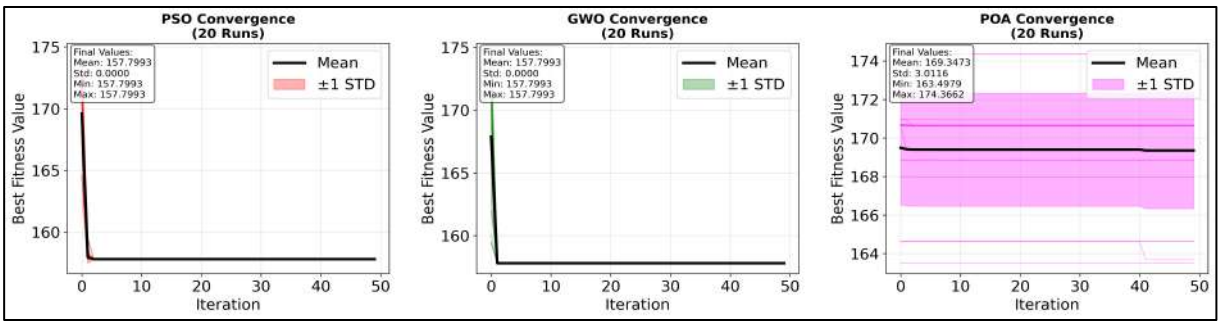

Figure 9. Comparison of the best fitness values of the PSO, GWO, and POA algorithms in optimizing the operation of a small-scale PV-PHS system in August 2023

The results of the convergence analysis of the optimization algorithm testing with PSO, GWO, and POA with 50 agents, 50 iterations, and multiple runs 20 times are presented in Figure 8. The convergence graph in Figure 8 demonstrates that the PSO and GWO algorithms yield an average fitness value of 157.7993 with a standard deviation of 0.00. Consequently, the minimum and maximum fitness values will be identical, specifically 157.7993. The POA algorithm yielded disparate results, exhibiting an average fitness value of 169.3473 and a standard deviation of 3.0116. Therefore, the minimum and maximum attainable fitness values are 163.4979 and 174.3662, respectively. The comparison of the average fitness convergence value with the standard deviation of the PSO, GWO, and POA algorithms is presented in the form of a box plot shown in Figure 9.

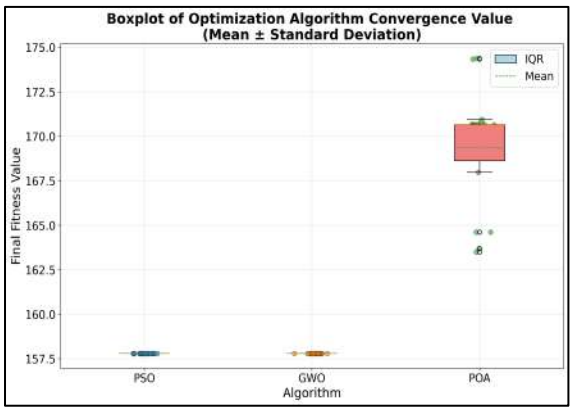

Figure 10. Boxplot of optimization convergence value (mean ± standard deviation) using PSO, GWO, and POA algorithms in optimizing the operation of a small-scale PV-PHS system in August 2023

Statistical Analysis of Second Scenario

Similar to the first scenario, statistical analysis in the second scenario was also conducted using the Wilcoxon Signed-Rank Test and the Mann-Whitney U Test. The results of the Wilcoxon Signed-Rank Test and the Mann-Whitney U Test are presented in Tables 6 and 7, respectively.

Table 6. Wilcoxon Signed-Rank Test Analysis for 2nd Scenario

Parame-ters	Comparison Algorithm		
	PSO-GWO	PSO-POA	GWO-POA
Wilcoxon Statistic	0.000000	0.000000	0.000000
P-Value	Nan	0.000087	0.000087
Significant	No	Yes	Yes
Better Algorithm	GWO	PSO	GWO
Median	PSO= 157.799303	PSO= 157.799303	GWO= 157.799303
	GWO= 157.799303	POA= 170.644403	POA= 170.644403

Table 7. Mann-Whitney U Test Analysis for 2nd Scenario

Parameters	Comparison Algorithm		
	PSO-GWO	PSO-POA	GWO-POA
Mann-Whitney	0.000000	5.410018	5.410018
P-Value	1.000000	0.000000	0.000000
Significant	No	Yes	Yes
Better Algorithm	GWO	PSO	GWO

Based on the data presented in Table 6, a comparative analysis of the performance of three optimization algorithms (PSO, GWO, and POA) can be conducted in two groups. The first group is a comparison of PSO with GWO, the second group is a comparison of POA with PSO and POA with GWO.

A comparison of the PSO and GWO algorithms reveals that there is no statistically significant difference between them. This is indicated by the undefined p-value (nan) and the Wilcoxon statistic of 0.000000, along with an identical median value (157.799303). Consequently, the performance of the two algorithms is statistically indistinguishable, although the superiority of the GWO algorithm is indicated by its superior parameter.

Meanwhile, in the comparison of PSO with POA and GWO with POA, a very significant difference is observed between the POA algorithm and the other two algorithms (PSO and

GWO). This is evidenced by the parameter p-value of 0.000087, which is far below the general significance level of 0.05. The median values indicate a marked superiority of both PSO and GWO compared to POA, which has a higher median value (170.644403). In the context of optimization, a lower median value is generally indicative of a superior solution. Therefore, it can be concluded that, statistically, the performance of PSO and GWO is equivalent, and both algorithms are significantly better than POA on the tested dataset or problem.

As evident in the statistical analysis employing the Wilcoxon Signed-Rank Test, the comparative analysis of the performance of three optimization algorithms using the Mann-Whitney U test also demonstrates a consistent pattern. A comparison of the PSO and GWO algorithms reveals that a p-value of 1.000000 signifies that the performance distributions of these algorithms are indistinguishable. While the output results indicate GWO as "better," the lack of statistical significance ($p > 0.05$) renders this difference statistically insignificant. This indicates that there is no statistically significant difference between PSO and GWO.

Meanwhile, a comparison of POA with PSO and POA with GWO reveals a p-value of 0.000000, which is significantly below the $\alpha = 0.05$ threshold. This outcome indicates a substantial discrepancy between POA and the other two algorithms. A comparative analysis reveals that both PSO and GWO demonstrate superior performance in comparison to POA. Therefore, it can be concluded that PSO and GWO have statistically equivalent performance, while both algorithms are significantly better than POA on the tested dataset.

The results of the PSO optimization process demonstrated a 9.59% increase in the average PHS generator output power, rising from a baseline of 12.41 watts to a maximum of 13.60 watts. The findings of this study indicate an augmentation in PHS generator energy, amounting to 8.54% from a baseline value of 9,321 kWh to 10,117 kWh. In the context of LPSP values, the application of PSO-based optimization successfully reduced the baseline value from 13.70% to 13.44%, indicating a decrease of 1.89%. Furthermore, the implementation of the PSO algorithm led to a reduction in the LOLE value from 399 hours in the baseline conditions to 391 hours, and the EENS value from 34,374 kWh to 44,489 kWh. However, PSO optimization, which was found to enhance the power of the PHS generator, had a consequential impact on the carbon footprint value. The value increased from the baseline condition value of 2.09 $kgCO_2e$ to 2.57 $kgCO_2e$, representing a 22.97% rise.

The experimental results demonstrate that the average output power of the PHS generator, when operated with the GWO algorithm, is equivalent to the PSO algorithm, which is 13.60 watts. Consequently, the total energy produced by the PHS generator is 10,117 kWh. In a similar vein, the reliability metric parameters, such as LPSP, LOLE, EENS, and carbon footprint, exhibited equivalent values to the optimization outcomes attained by the PSO algorithm.

The system optimization performance analysis employing the POA algorithm demonstrates an average of PHS generator power gain of 13 watts, a 4.85% increase from the baseline value (12.41 watts). Consequently, the total energy produced by the PHS generator is 9,679 kWh, with a total stored energy of 115,602 kWh. The reliability indicators of the LPSP system obtained by the POA algorithm are 11.57%, LOLE 395 hours, and EENS 44,927 kWh. Meanwhile, the carbon footprint value resulting from the POA algorithm optimization is 2.30 kgCO2e. The threshold values for the pump and the generator, as determined by the POA algorithm optimization, are 33.23 watts and 65.30 watts, respectively.

C. Comparative Analysis of the Optimization Algorithm on First and Second Scenario

As illustrated in Table 9, a comparative analysis of the performance of the PSO, GWO, and WOA algorithms is presented for the average value parameters derived from the first and second scenario test results. It is noteworthy that each scenario is representative of distinct weather conditions, namely the rainy season and

Table 8. A comparative analysis of power, energy, and operating performance metrics of small-scale PV-PHS systems was conducted in August of 2023.

System	Total PV energy (kWh)	Total PHS energy (kWh)	Total Stored Energy (kWh)	LPSP (%)	LOLE (hours)	EENS (kWh)	Carbon ($kgCO_2e$)
Baseline	638.917	9.231	**115.366**	13.70	399	45.374	**2.09**
PSO	638.917	**10.117**	114.937	**13.44**	**391**	**44.489**	2.57
GWO	638.917	**10.117**	114.937	**13.44**	**391**	**44.489**	2.57
POA	638.917	9.795	114.066	13.53	394	44.811	2.36

Table 9. A Comparative analysis of average power, energy, and operational performance metrics of small-scale PV-PHS systems (January and August 2023).

System	Average of Total PV energy (kWh)	Average of Total PHS energy (kWh)	Average of Total Stored Energy (kWh)	Average of LPSP (%)	Average of LOLE (hours)	Average of EENS (kWh)	Average of Carbon ($kgCO_2e$)	Pump & Generator threshold [Watt]
Baseline	476.553	8.804	96.207	19.36	470	64.103	**2.04**	[100, 100]
PSO	476.553	**10.225**	97.761	**18.93**	**458**	**62.682**	2.55	[0, 6]
GWO	476.553	**10.225**	97.761	**18.93**	**458**	**62.682**	2.55	[0, 20]
POA	476.553	9.572	**98.166**	19.13	468	63.335	2.28	[33, 65]

dry season, respectively. As demonstrated in Table 9, it can be concluded that the PSO and GWO algorithms demonstrate equivalent performance metrics and exhibit superiority over the POA algorithm in terms of the average total energy parameters of the PHS, LPSP, LOLE, and EENS generators. Concurrently, the POA algorithm engenders a comparatively augmented mean total energy storage value in contrast to the PSO and GWO algorithms.

D. Comparative Analysis of PV-PHS System with PV-Battery, PV-Grid, and PV-Diesel Systems

A comparative analysis was conducted to evaluate the performance of the PV-PHS system in terms of both reliability metrics and environmental aspects. The analysis was conducted with systems of the same capacity for off-grid PV-battery system configurations, PV-grid system configurations, and PV-diesel system configurations. The calculation of performance parameters and carbon footprint necessitates the establishment of appropriate assumptions for each comparison system.

In the operation of the PV-battery system, the embodied carbon value is a significant factor, although it is not the sole determining element. The battery's life cycle, capacity, and DoD value also play a significant role in the overall assessment. The battery's embodied carbon value was determined to be 80 $kgCO_2/kWh$, and the battery capacity and DoD value were established at 10 kWh and 80%, respectively. During the one-month in January and August 2023 PV-Battery system operation test, a total carbon footprint of 1064.25 $kgCO_2e$ and 1172.70 kgCO2e, respectively. Meanwhile, the carbon intensity is 3,652 kg/kWh and 4,024 kg/kWh for the energy distributed, respectively.

In the context of PV-grid systems, the calculation of the carbon footprint is influenced by the grid carbon intensity value, which is multiplied by the net energy of the grid. The net energy of the grid is defined as the energy imported from the grid minus the energy exported to the grid. In instances where photovoltaic (PV) energy is inadequate, the system draws upon the grid for supplemental power. Conversely, when PV energy production exceeds demand, the surplus PV energy is dispatched to the grid, thereby reducing the grid's reliance on activated carbon. Assuming a grid carbon value of 0.4 $kgCO_2e/kWh$, the results of testing the operation of the PV-grid system over the course of one month in January and August 2023, resulted in a total carbon footprint of 12890.88 $kgCO_2e$ and 8073.05 $kgCO_2e$, respectively. Meanwhile, the carbon intensity is 44,238 kg/kWh and 27,704 kg/kWh for the energy distributed, respectively.

Subsequently, a comparison will be made with the PV-diesel system. Diesel is typically employed when the energy output from PV is inadequate. The carbon footprint value of the PV-diesel system is determined by two factors. Firstly, the carbon footprint of diesel when active, which is 0.82 $kgCO_2e/kWh$. Secondly, the efficiency of the diesel generator. Assuming an efficiency rating of 30% for the diesel generator, the carbon footprint of the PV-diesel system operation is proportional to the electrical energy produced, multiplied by the result of dividing the diesel carbon footprint by the efficiency rating of the diesel generator. The results of the PV-diesel

Figure 10. Comparison between PV-PHS, PV-Battery, PV-grid, and PV-Diesel over a period of one week (7 days) (a) total carbon footprint, (b) carbon intensity per kWh delivered

System	LPSP		Carbon Footprint (kg CO_2 e)		Carbon Intensity (kg/kWh)	
	January	August	January	August	January	August
PV-PHS	25.01	13.70	1.99	2.09	0.007	0.007
PV-Battery	15.36	0	1064.24	1172.70	3.652	4.024
PV-Grid	0	0	12890.88	8073.05	44.238	27.704
PV-Diesel	0	0	7550374.25	4728498.67	25910.687	16226.831

system operation test, which spanned one month in January and August 2023. Meanwhile, the carbon intensity value of the PV-Diesel system was obtained as 25910.687 kg/kWh for January and 16226.831 for August. The results of the performance comparison of the PV-PHS system with the PV-battery, PV-grid, and PV-Diesel systems are presented in full in Table 10.

IV. CONCLUSION

This paper discusses the application of Particle Swarm Optimization (PSO), Grey Wolf Optimization (GWO), and Puzzle Optimization Algorithms (POA) to optimize the operation of Pumped Hydro Storage (PHS) in small-scale Photovoltaic (PV) systems in high-rise buildings. This optimization aims to minimize the Loss of Power Supply Probability (LPSP) and carbon footprint. Simulation test results show that the optimization algorithms, especially PSO and GWO, have a small impact on the performance improvement of small-scale PV-PHS systems.

The findings of the study, which employed the January weather dataset to model the rainy season, revealed that the performance of the small-scale PV-PHS system, both in baseline conditions and following optimization, resulted in a lower total PHS generator energy and stored power compared to the test conducted in August, which represented the characteristics of the summer. The system reliability parameter values for both LPSP, LOLE, and EENS also exhibited higher results (lower performance) compared to the test results with August data.

While small-scale PV-PHS systems generally exhibit a reduced carbon footprint relative to PV-battery, PV-grid, and PV-diesel systems, they nevertheless possess inherent system reliability limitations, with a performance that falls below the 10% threshold of the optimal value for a stand-alone PV system. The PV-PHS system's suboptimal size, in terms of capacity, has a considerable impact on system performance.

Based on these conditions, future work can include optimizing the size of a more ideal small-scale PV-PHS system to achieve a system reliability parameter (LPSP) value of less than or equal to 10% while maintaining a relatively low carbon footprint. Furthermore, hybrid optimization algorithms can be tested to achieve optimal optimization results.

ACKNOWLEDGMENT

The authors would like to express their gratitude to the Indonesian Ministry of Education, Culture, Research, and Technology for the funding provided for the implementation of this research activity under the regular fundamental research grant (PFR) scheme.

REFERENCES

[1] A. Bagaskara *et al.*, “Indonesia Energy Transition Outlook 2023: Tracking Progress of Energy Transition in Indonesia: Pursuing Energy Security in the Time of Transition.,” 2023. Available Online: https://iesr.or.id/en/pustaka/indonesia-energy-transition-outlook-ieto-2023/.

[2] I. Akhtar, S. Kirmani, M. Jameel, and F. Alam, “Feasibility Analysis of Solar Technology Implementation in Restructured Power Sector with Reduced Carbon Footprints,” *IEEE Access*, vol. 9, pp. 30306–30320, 2021, doi: 10.1109/ACCESS.2021.3059297.

[3] P. Chaudhary and M. Rizwan, “Energy management supporting high penetration of solar photovoltaic generation for smart grid using solar forecasts and pumped hydro storage system,” *Renew. Energy*, vol. 118, pp. 928–946, 2018, doi: 10.1016/j.renene.2017.10.113.

[4] A. Setas Lopes, R. Castro, and C. S. Silva, “Design of water pumped storage systems: A sensitivity and scenario analysis for island microgrids,” *Sustain. Energy Technol. Assessments*, vol. 42, no. June, p. 100847, 2020, doi: 10.1016/j.seta.2020.100847.

[5] M. S. Javed, T. Ma, J. Jurasz, and M. Y. Amin, “Solar and wind power generation systems with pumped hydro storage: Review and future perspectives,” *Renew. Energy*, vol. 148, pp. 176–192, 2020, doi: 10.1016/j.renene.2019.11.157.

[6] N. Mousavi, G. Kothapalli, D. Habibi, C. K. Das, and A. Baniasadi, “A novel photovoltaic-pumped hydro storage microgrid applicable to rural areas,” *Appl. Energy*, vol. 262, no. February, p. 114284, 2020, doi: 10.1016/j.apenergy.2019.114284.

[7] G. de Oliveira e Silva and P. Hendrick, “Pumped hydro energy storage in buildings,” *Appl. Energy*, vol. 179, pp. 1242–1250, 2016, doi: 10.1016/j.apenergy.2016.07.046.

[8] S. Lin, T. Ma, and M. Shahzad Javed, “Prefeasibility study of a distributed photovoltaic system with pumped hydro storage for residential buildings,” *Energy Convers. Manag.*, vol. 222, no. February, p. 113199, 2020, doi: 10.1016/j.enconman.2020.113199.

[9] K. Sun, K. Li, J. Pan, Y. Liu, and Y. Liu,

"An optimal combined operation scheme for pumped storage and hybrid wind-photovoltaic complementary power generation system," *Appl. Energy*, vol. 242, no. June 2018, pp. 1155–1163, 2019, doi: 10.1016/j.apenergy.2019.03.171.

[10] T. Alquthami, S. Ehsan, and M. Faizan, "Short-term optimal scheduling of hydro-thermal power plants using artificial bee colony algorithm," *Energy Reports*, vol. 6, pp. 984–992, 2020, doi: 10.1016/j.egyr.2020.04.003.

[11] P. Afzali, N. Anjom, M. Rashidinejad, and A. Bakhshai, "Techno-economic study driven based on available efficiency index for optimal operation of a smart grid in the presence of energy storage system," *J. Energy Storage*, vol. 32, no. August, p. 101853, 2020, doi: 10.1016/j.est.2020.101853.

[12] S. Makhdoomi and A. Askarzadeh, "Optimizing operation of a photovoltaic / diesel generator hybrid energy system with pumped hydro storage by a modi fi ed crow search algorithm," *J. Energy Storage*, vol. 27, no. October 2019, p. 101040, 2020, doi: 10.1016/j.est.2019.101040.

[13] W. L. Schram, T. Alskaif, I. Lampropoulos, S. Henein, and W. G. J. H. M. Van Sark, "On the Trade-Off Between Environmental and Economic Objectives in Community Energy Storage Operational Optimization," *IEEE Trans. Sustain. Energy*, vol. 11, no. 4, pp. 2653–2661, 2020, doi: 10.1109/TSTE.2020.2969292.

[14] M. W. Khan, J. Wang, and L. Xiong, "Optimal energy scheduling strategy for multi-energy generation grid using multi-agent systems," *Int. J. Electr. Power Energy Syst.*, vol. 124, no. June 2020, p. 106400, 2021, doi: 10.1016/j.ijepes.2020.106400.

[15] N. Mousavi, G. Kothapalli, D. Habibi, and S. W. Lachowicz, "A real-time energy management strategy for pumped hydro storage systems in farmhouses," *J. Energy Storage*, vol. 32, no. September, p. 101928, 2020, doi: 10.1016/j.est.2020.101928.

[16] B. A. Bhayo, H. H. Al-kayiem, S. I. U. Gilani, and F. B. Ismail, "Power management optimization of hybrid solar photovoltaic-battery integrated with pumped-hydro-storage system for standalone electricity generation," *Energy Convers. Manag.*, vol. 215, no. February, p. 112942, 2020, doi: 10.1016/j.enconman.2020.112942.

[17] C. Li, X. Jia, Y. Zhou, and X. Li, "A microgrids energy management model based on multi-agent system using adaptive weight and chaotic search particle swarm optimization considering demand response," *J. Clean. Prod.*, vol. 262, p. 121247, 2020, doi: 10.1016/j.jclepro.2020.121247.

[18] N. Rezaei, M. Mazidi, M. Gholami, and M. Mohiti, "A new stochastic gain adaptive energy management system for smart microgrids considering frequency responsive loads," *Energy Reports*, vol. 6, pp. 914–932, 2020, doi: 10.1016/j.egyr.2020.04.021.

[19] G. A. M. Castorino *et al.*, "Optimization of sizing and operation of pumped hydro storage plants under current and future economic scenarios," *J. Energy Storage*, vol. 119, no. March, 2025, doi: 10.1016/j.est.2025.116130.

[20] S. Zhu, E. Wang, S. Han, and H. Ji, "Optimal Scheduling of Combined Heat and Power Systems Integrating Hydropower-Wind-Photovoltaic-Thermal-Battery Considering Carbon Trading," *IEEE Access*, vol. 12, no. July, pp. 98393–98406, 2024, doi: 10.1109/ACCESS.2024.3429399.

[21] Z. Zhu, X. Wang, C. Jiang, L. Wang, and K. Gong, "Multi-objective optimal operation of pumped-hydro-solar hybrid system considering effective load carrying capability using improved NBI method," *Int. J. Electr. Power Energy Syst.*, vol. 129, no. January, 2021, doi: 10.1016/j.ijepes.2021.106802.

[22] S. Yadav, P. Kumar, and A. Kumar, "Grey wolf optimization based optimal isolated microgrid with battery and pumped hydro as double storage to limit excess energy," *J. Energy Storage*, vol. 74, no. April, 2023, doi: 10.1016/j.est.2023.109440.

[23] B. Chegari, M. Tabaa, E. Simeu, and M. El Ganaoui, "Optimal energy management of a hybrid system composed of PV, Wind turbine, pumped hydropower storage and battery storage to achieve a complete energy self-sufficiency in residential buildings," *IEEE Access*, vol. 12, no. July, pp. 126624–126639, 2024, doi: 10.1109/ACCESS.2024.3454149.

[24] T. R. Simon, D. Inman, R. Hanes, G. Avery, D. Hettinger, and G. Heath, "Life Cycle Assessment of Closed-Loop Pumped Storage Hydropower in the

United States," *Environ. Sci. Technol.*, vol. 57, no. 33, pp. 12251–12258, 2023, doi: 10.1021/acs.est.2c09189.

[25] S. Mirjalili, S. M. Mirjalili, and A. Lewis, "Grey Wolf Optimizer," *Adv. Eng. Softw.*, vol. 69, pp. 46–61, 2014, doi: 10.1016/j.advengsoft.2013.12.007.

[26] F. A. Zeidabadi and M. Dehghani, "POA: Puzzle Optimization Algorithm," *Int. J. Intell. Eng. Syst.*, vol. 15, no. 1, pp. 273–281, 2022, doi: 10.22266/IJIES2022.0228.25.